near the slot exit. During the suction phase (instants B, C, and D), the fluid particles in the near-wall region of the boundary layer upstream of the slot exit flow into the slot. The fluid particles in the region farther from the wall, which are momentum rich, pass over the slot exit and move down to the near-wall region of the boundary layer downstream of the slot exit. As a result, the boundary-layer velocity profiles downstream of the slot exit become fuller and more separation resistant. During the blowing phase (instants F, G, and H), the major effect of the blowing is to make the boundary-layer velocity profile downstream of the slot exit fuller. When the velocity-vector plots at instants F, G, and H (blowing phase) are compared with that at instants B, C, and D (suction phase), it is clearly seen that the boundary-layer velocity profiles during the suction phase are fuller than that during the blowing phase. The reason for this is that the suction not only removes the near-wall retarded fluid particles but also brings fluid particles that are momentum rich to the near-wall region.

The effect of varying V_a while keeping f the same as that of case 1 was studied. When V_a is decreased to 1, the separation is delayed, but it is not suppressed. As a result, $\bar{C}_L$ is only 0.72. When V_a is increased to 2, separation is completely suppressed, and $\bar{C}_L$ is as large as 2.2. From these results, it is seen that for the present airfoil at this f, at least a value of 1.5 is needed for V_a to suppress the flow separation.

The effect of varying f while keeping V_a as in case 1 was also studied. When f is increased to 10, similar to case 1, the global flowfield almost does not vary with time, and the separation is suppressed to almost the same extent as in case 1. The amplitudes of C_L and C_D, and also $\bar{C}_L$ and $\bar{C}_D$, are very close to that of case 1. When f is decreased to 1, the global flowfield becomes slightly unsteady. When f is further decreased to 0.25, the global flowfield is noticeably unsteady, varying with time periodically with the same period as that of the V. In part of the cycle, the flow is separated, and in another part of the cycle, the flow is well controlled. The amplitudes of the C_L and C_D variations are much larger than that of case 1 (C_L varies between 0.73 and 1.63). The described flow behavior is because, for the same mass flux, suction is more effective than blowing in controlling boundary-layer separation. When suction and blowing are applied alternatively at very low frequency and the blowing is not strong enough for suppressing the separation, alternating attached and separated flows would occur.

Conclusions

1) By the use of ATBS, in both the blowing and suction phases, the boundary-layer velocity profiles downstream of the slot are made fuller and more separation resistant.

2) For the airfoil considered in the Note, when the frequency and amplitude of the blowing/suction are above 1 and 1.5, respectively, the flow separation is suppressed. The global flowfield does not vary with time. The flow in the neighborhood of the slots varies with time, and as a result, the aerodynamic forces oscillate with small amplitudes.

3) The suction is more effective than the blowing in controlling the boundary-layer separation, and as a result, when the frequency of the blowing/suction is low, the global flowfield would vary with time periodically with the same period as that of the blowing/suction and the aerodynamic forces would oscillate with large amplitudes.

References

[1]Gad-el-Hak, M., and Bushnell, D. M., "Separation Control: Review," *Journal of Fluid Engineerings*, Vol. 113, No. 3, 1991, pp. 5–29.

[2]Wang, C. Y., and Sun, M., "Separation Control on a Thick Airfoil with Multiple Slots Blowing at Small Speeds," *Acta Mechanica*, Vol. 143, No. 3–4, 2000, pp. 215–227.

[3]Beam, R. M., and Warming, R. F., "An Implicit Factored Scheme for the Compressible Navier–Stokes Equations," *AIAA Journal*, Vol. 16, No. 4, 1978, pp. 393–402.

[4]Baldwin, B., and Lomax, H., "Thin-Layer Approximation and Algebraic Model for Separated Turbulent Flows," AIAA Paper 78-0257, Jan. 1978.

M. Samimy
Associate Editor

Effect of Wall Shear Stress on Structural Vibration

Abdelkader Frendi*
University of Alabama in Huntsville, Huntsville, Alabama 35899

Nomenclature

D	=	beam stiffness given by $D = E_p h^3/12(1-\nu^2)$
E_p	=	modulus of elasticity
h	=	beam thickness
L	=	beam length
M_∞	=	freestream Mach number
P	=	total mean pressure
P^a	=	acoustic pressure
P^{bl}	=	turbulent boundary-layer pressure
Re_L	=	freestream Reynolds number
t	=	time
U	=	nondimensional mean velocity
x	=	downstream coordinate direction
z	=	vertical coordinate direction
Γ	=	structural damping
ΔP	=	pressure difference across the beam
ε	=	amplitude of the inflow excitation
η	=	out-of-plane beam displacement
μ	=	molecular viscosity of the fluid
ν	=	Poisson's ratio of the beam material
ξ	=	in-plane beam displacement
ρ_p	=	beam density
τ_w	=	fluid wall shear stress
ω_0	=	frequency of the inflow excitation

Introduction

FLUID wall shear stress has not been included in most structural vibration models.[1–7] In this Note, a fully coupled model that accounts for all fluid–structure interactions is presented. The system of equations describing the motion of a beam is derived from the fundamental principles and shows explicitly the fluid wall shear stress. In addition, a simple beam equation that takes into account the wall shear stress is derived using an integrated value of the tension over the beam.

Full coupling of structural vibration to the surrounding fluid has been shown to be critical in several earlier studies. Frendi and Robinson[8] showed that for large-amplitude harmonic or random excitations, a fully coupled model was able to explain some of the results obtained in an earlier experimental study.[9] An attempt at explaining the same experimental results using a decoupled structural vibration model failed. In another experimental and numerical study, Maestrello et al.[10] showed that, when a flat panel was excited by plane acoustic waves having a frequency that corresponds to one of the panel's natural frequencies, its response became nonlinear as the amplitude of the excitation was increased. Similar results were later obtained by Frendi et al.[11] using a two-dimensional fully coupled model. The fluid was modeled using the nonlinear Euler equations, whereas the structure was modeled using a nonlinear beam equation. Wall shear stress was not needed in the model because the experiment was carried out in a transmission loss facility (no flow).

In more recent studies, Frendi[12,13] used the fully coupled model to study the noise transmission from a supersonic turbulent boundary layer to an interior cavity through a flexible structure. The model did not include the effects of the fluid wall shear stress on the structural

Received 13 March 2000; revision received 5 October 2000; accepted for publication 29 November 2000.

*Associate Professor, Mechanical and Aerospace Engineering Department, TH N264. Senior Member AIAA.

vibration. The results compared well with those obtained in the wind tunnel[14] and showed the importance of full coupling. In this Note, the same fluid model derived in Refs. 12 and 13 is used to simulate the turbulent boundary layer. However, the beam equation is modified to account for the fluid wall shear stresses.

The fully coupled model is described in the next section. It is followed by a brief description of the various numerical solution techniques used. The results are then discussed, followed by the conclusions.

Mathematical Model

Consider a beam, which is in contact with a fluid flow on one side (Fig. 1). The balance of forces on a beam element in the z direction leads to

$$D\frac{\partial^4\eta}{\partial x^4} + \rho_p h\frac{\partial^2\eta}{\partial t^2} - N_x\frac{\partial^2\eta}{\partial x^2} - \frac{\partial}{\partial x}\left[\tau_w\left(\eta + \frac{h}{2}\right)\right] + \Gamma\frac{\partial\eta}{\partial t} = \Delta P \tag{1}$$

and that in the x direction gives

$$\rho_p h\frac{\partial^2\xi}{\partial t^2} - \frac{\partial N_x}{\partial x} + \Gamma\frac{\partial\xi}{\partial t} = \tau_w \tag{2}$$

with

$$N_x = E_p h\left[\frac{\partial\xi}{\partial x} + \frac{1}{2}\left(\frac{\partial\eta}{\partial x}\right)^2\right] \tag{3}$$

In the absence of wall shear stress and neglecting the in-plane acceleration, the beam equation becomes

$$D\frac{\partial^4\eta}{\partial x^4} + \rho_p h\frac{\partial^2\eta}{\partial t^2} - \bar{N}_x\frac{\partial^2\eta}{\partial x^2} + \Gamma\frac{\partial\eta}{\partial t} = \Delta P \tag{4}$$

where $\bar{N}_x$ is given by

$$\bar{N}_x = \frac{E_p h}{2L}\int_0^L \left(\frac{\partial\eta}{\partial x}\right)^2 \mathrm{d}x \tag{5}$$

Equation (5) is obtained by integration of Eq. (3) subject to the fixed-end condition. Equations (4) and (5) are used extensively in the literature, whereas Eqs. (1–3) are rarely used. In the presence of wall shear stress, instead of using the system of coupled equations (1–3), a simplified equation derived using Eq. (5) is also used:

$$D\frac{\partial^4\eta}{\partial x^4} + \rho_p h\frac{\partial^2\eta}{\partial t^2} - \bar{N}_x\frac{\partial^2\eta}{\partial x^2} - \frac{\partial}{\partial x}\left[\tau_w\left(\eta + \frac{h}{2}\right)\right] + \Gamma\frac{\partial\eta}{\partial t} = \Delta P \tag{6}$$

From here onward, the beam model described by Eq. (6) will be referred to as the global-N_X model, whereas the one given by Eqs. (1–3) will be the local-N_x model.

Equations (1–6) are coupled to the fluid flow equations given by the conditionally averaged Navier–Stokes equations derived in Refs. 12 and 13. The wall shear stress used in Eq. (1) is obtained from the flow solution using

$$\tau_w = \mu\left.\frac{\partial U}{\partial z}\right|_{z=0} \tag{7}$$

and in Eqs. (1), (4), and (6), ΔP is given by

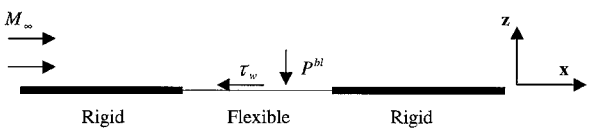

Fig. 1 Physical boundaries of the computational domain.

$$\Delta P = P^a - P^{\mathrm{bl}} \tag{8}$$

where P^a is constant and equal to the freestream pressure (in Refs. 12 and 13 Kirchhoff's formula, derived in Ref. 15, was used to obtain P^a) and P^{bl} is the pressure obtained from the turbulent boundary layer.

Method of Solution

The turbulent boundary-layer equations are solved using the two-dimensional thin-layer version of the three-dimensional Navier–Stokes code CFL3D.[16] The numerical method uses a second-order accurate finite volume scheme. The convective terms are discretized with an upwind scheme that is based on the Roe's flux difference splitting method, whereas all of the viscous terms are centrally differenced. The equations are integrated in time with an implicit, spatially split approximate factorization scheme. The thin-layer approximation retains only those viscous terms with derivatives normal to the body surface. This is generally considered to be a good approximation for high Reynolds number aerodynamic flows with minimal separation. The beam equations (1–6) are integrated using an implicit finite difference method for structural dynamics developed by Hoff and Pahl.[17] Mean flow disturbances are introduced at the inflow boundary in the form of

$$u = U + \varepsilon\sin(\omega_0 t) \tag{9}$$

where ω_0 is chosen to correspond to one of the natural frequencies of the vibrating plate and ε is a nondimensional amplitude and is varied between 0.05 and 0.4.

The coupling between the flow and the structure is achieved by forcing the vertical velocity of the fluid at the wall to be equal to

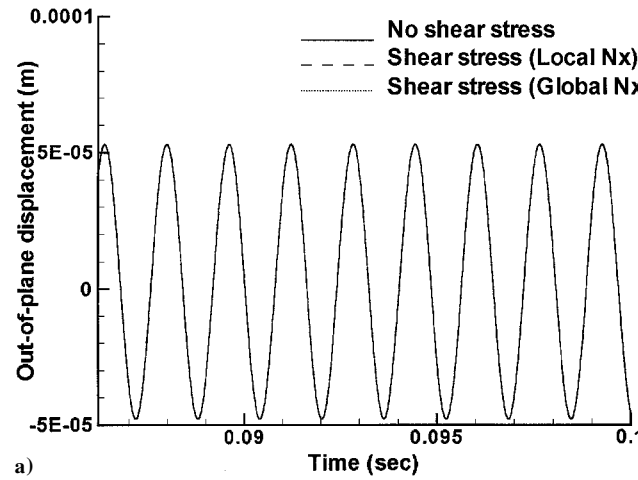

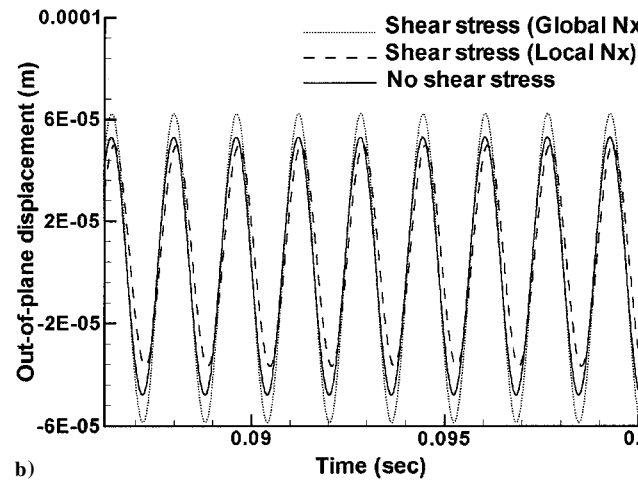

Fig. 2 Time histories of the out-of-plane vibration response at the beam center for a) $\varepsilon = 0.05$ and τ_w and b) $\varepsilon = 0.05$ and $100 \times \tau_w$.

that of the vibrating beam. In turn, the fluid wall shear stress and pressure are used to compute the beam response. This procedure is repeated at each time step.

Results and Discussion

The freestream fluid conditions used are Mach number 2.4, temperature 311.11 K, and Reynolds number per meter 9.843×10^6 (these freestream conditions are the same as those used in Refs. 12 and 13). The beam properties are thickness $h = 5.08 \times 10^{-4}$ m, length $L = 0.254$ m, stiffness $D = 2.0$ N · m, density per unit area $\rho_p h = 2.714$ kg/m^2, Poisson's ratio $\nu = 0.3$, and physical damping $\Gamma = 15.5$ N · s/m^3. The first six natural frequencies of the beam are 47.5, 130.1, 254.0, 417.9, 620.7, and 861.0 Hz. An excitation frequency of 620.7 Hz is used to excite one resonant mode of the beam. Two values of ε, 0.05 (linear case) and 0.4 (nonlinear case), are used to carry out several fully coupled computations. The computational domain is 0.61 m long and 0.305 m high with 101×81 grid points in the respective directions.

For the small value of ε, 0.05, the out-of-plane displacement responses given by all of the beam models are the same as shown in Fig. 2a. The time history of the displacement response at the center of the beam indicates a linear response. This result is expected because, for small excitation amplitudes, the wall shear stress term and the curvature term are small. To simulate the effects of a flow with strong wall shear stress component and low-pressure loading, the same value of ε is used, and the wall shear stress is artificially increased by a factor of a 100 (this may be the case in separated flows). Figure 2b shows a comparison of the results obtained by the local-N_x and global-N_x models to those obtained when the shear stress term is neglected. Compared to the no-shear case, the results given by the local-N_x model show decreased vibration amplitudes and a slight phase shift, whereas those obtained using the global-N_x model show increased vibration amplitudes and no phase shift.

When ε is increased to 0.4, Fig. 3a shows no difference between the time histories given by all models, suggesting a negligible effect of wall shear stress for the flow conditions being studied. This conclusion supports the results published in Refs. 12 and 13, which were obtained without wall shear stress. To enhance the effects of wall shear stress on the beam response at high-pressure loading, the value of ε is kept constant and equal to 0.4 while wall shear stress is increased by a factor of 100. Figure 3b shows the beam response obtained using the three models. Just as in the case of low-pressure loading, the time history obtained using the local-N_x model shows

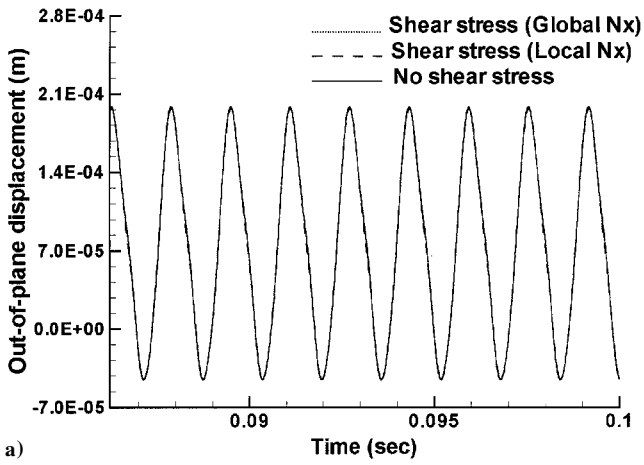

a)

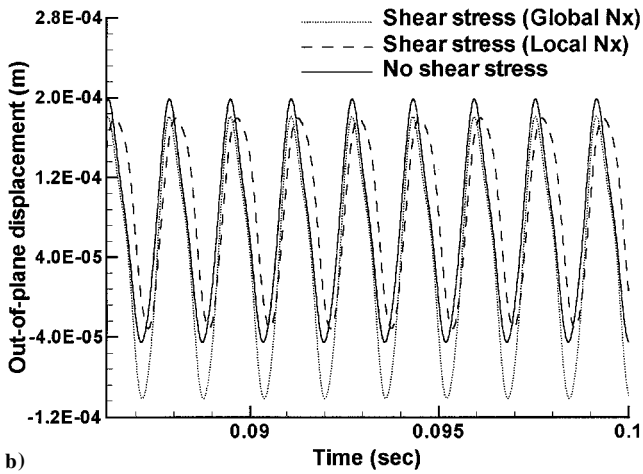

b)

Fig. 3 Time histories of the out-of-plane vibration response at the beam center for a) $\varepsilon = 0.4$ and τ_w and b) $\varepsilon = 0.4$ and $100 \times \tau_w$.

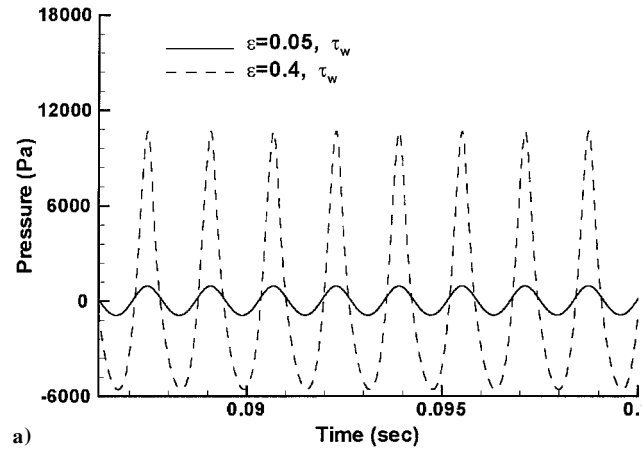

a)

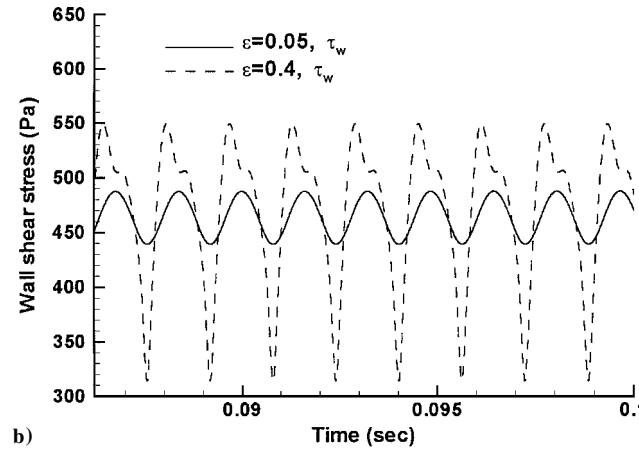

b)

Fig. 4 Time histories at the center of the beam of a) surface pressure and b) wall shear stress.

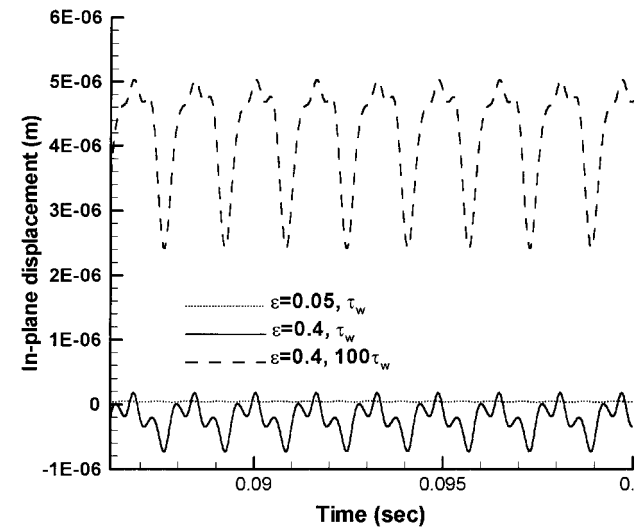

Fig. 5 Time histories of the in-plane displacement response at the center of the beam.

reduced vibration amplitudes and a slight phase shift. However, the global-N_x model results show no phase shift and an increased vibration amplitude. Figure 4a shows the time history of the surface pressure for the two ε cases studied, 0.05 and 0.4, using the computed value of τ_w. Increasing ε results in increased surface pressure amplitudes and nonsymmetric fluctuations. Figure 4b shows the time histories of the wall shear stress. Similar to the pressure, the shear stress amplitudes increase with increasing ε and show the presence of additional frequencies. The increase in amplitudes is not as large as in the case of the pressure. Figure 5 shows the in-plane displacement response at the center of the beam for the same two cases and for the case with large wall shear stress and $\varepsilon = 0.4$. In all of the cases, the time histories show the presence of more than one frequency. As expected, the in-plane displacement response is orders of magnitude smaller than the out-of-plane one.

Conclusions

Results obtained in this study show that in flows producing large wall shear stresses, a fully coupled model that uses the local value of the tension, that is, a local-N_x model, and that accounts for wall shear stress is needed for accurate predictions of structural response. This result was shown to be true for both low- and high-pressure loading. In flows with low wall shear stresses, the global-N_x model is sufficient for accurate structural vibration predictions.

References

[1]Corcos, G. M., "Resolution of Pressure in Turbulence," *Journal of the Acoustical Society of America*, Vol. 35, No. 2, 1963, pp. 192–198.

[2]Chase, D. M., "Modeling the Wavenumber-Frequency Spectrum of Turbulent Boundary Layer Wall Pressure," *Journal of Sound and Vibration*, Vol. 70, No. 1, 1980, pp. 29–67.

[3]Leganelli, A. L., and Wolfe, H., "Prediction of Fluctuating Pressure in Attached and Separated Turbulent Boundary Layer Flow," AIAA Paper 89-1064, 1989.

[4]Efimtsov, B. M., "Characteristics of the Field of Turbulent Wall Pressure Fluctuations at Large Reynolds Numbers," *Soviet Physical Acoustics*, Vol. 28, No. 4, 1982, pp. 289–292.

[5]Graham, W. R., "A Comparison of Models for Wavenumber Frequency Spectrum of Turbulent Boundary Layer Pressures," *Proceedings of the First AIAA/CEAS Conference on Aeroacoustics* AIAA, Washington, DC, 1994, pp. 711–720.

[6]Vacaitis, R., Jan, C. M., and Shinozuka, M., "Nonlinear Panel Response from a Turbulent Boundary Layer," *AIAA Journal*, Vol. 10, No. 7, 1972, pp. 895–899.

[7]Wu, S. F., and Maestrello, L., "Responses of Finite Baffled Plate to Turbulent Flow Excitations," *AIAA Journal*, Vol. 33, No. 1, 1995, pp. 13–19.

[8]Frendi, A., and Robinson, J., "Effect of Acoustic Coupling on Random and Harmonic Plate Vibrations," *AIAA Journal*, Vol. 31, No. 11, 1993, pp. 1992–1997.

[9]Robinson, J., Rizzi, S., Clevenson, S., and Daniels, E., "Large Deflection Random Response of Flat and Blade Stiffened Carbon–Carbon Panels," AIAA Paper 92-2390, 1992.

[10]Maestrello, L., Frendi, A., and Brown, D. E., "Nonlinear Vibration and Radiation from a Panel with Transition to Chaos Induced by Acoustic Waves," *AIAA Journal*, Vol. 30, No. 11, 1992, pp. 2632–2638.

[11]Frendi, A., Maestrello, L., and Bayliss, A., "Coupling Between Plate Vibration and Acoustic Radiation," *Journal of Sound and Vibration*, Vol. 177, No. 2, 1994, pp. 207–226.

[12]Frendi, A., "Coupling Between a Supersonic Turbulent Boundary Layer and a Flexible Structure," *AIAA Journal*, Vol. 35, No. 1, 1997, pp. 58–66.

[13]Frendi, A., "Effect of Pressure Gradients on Plate Response and Radiation in a Supersonic Turbulent Boundary Layer," NASA CR-201691, 1997.

[14]Maestrello, L., "Radiation from and Panel Response to a Supersonic Turbulent Boundary Layer," *Journal of Sound and Vibration*, Vol. 10, No. 2, 1969, pp. 262–295.

[15]Frendi, A., Maestrello, L., and Ting, L., "An Efficient Model for Coupling Structural Vibrations with Acoustic Radiation," *Journal of Sound and Vibration*, Vol. 182, No. 5, 1995, pp. 741–757.

[16]Rumsey, C., Thomas, J., Warren, G., and Liu, G., "Upwind Navier–Stokes Solutions for Separated Periodic Flows," AIAA Paper 86-0247, 1986.

[17]Hoff, C., and Pahl, P. J., "Development of an Implicit Method with Numerical Dissipation from a Generalized Single-Step Algorithm for Structural Dynamics," *Computer Methods in Applied Mechanics and Engineering*, Vol. 67, No. 2, 1988, pp. 367–385.

E. Livne
Associate Editor

Absolute Instability of a Potential Flow over Plate–Spring System

Zhao Hanzhong*
Huazhong University of Science and Technology, 430074 Wuhan, People's Republic of China
and
K. S. Yeo†
National University of Singapore, 119260 Singapore, Republic of Singapore

Introduction

THE concept of using a compliant wall to reduce skin friction and flow noise has motivated a number of studies of instabilities that arise from the interaction between a passive compliant coating and a flow. In a series of experiments, Hansen et al.[1] and Gad-el-Hak et al.[2] observed the large-amplitude form of a static divergence (SD) wave on a highly damped viscoelastic layer under turbulent boundary layers. The onset of SD instability will lead to the temporal growth of the disturbance at any fixed point in the flow and is likely to give rise to significantly large surface vibrations or oscillations. This may cause a roughness effect that would directly increase the skin-friction drag and flow noise.

The SD instability mode is generally believed to be an absolute instability. The limited knowledge that we have of absolute instability over flexible plates has been derived primarily from a handful of works. For example, Brazier-Smith and Scott[3] found that potential flow over nondissipative compliant plates suffers from absolute instability when the flow speed exceeds a certain critical value, depending on the properties of the plate; Lucey and Carpenter[4] studied the response of a single-point pulse perturbation in an unsteady potential flow; and Yeo et al.[5,6] studied the absolute instability of laminar boundary layer and modified potential flows, representing turbulent and laminar boundary layers, over viscoelastic compliant layers.

The focus of the present Note is on uniform potential flow over a plate–spring system. Uniform potential flow represents the limiting form of laminar and turbulent boundary layers as their thickness tends to zero, and the plate–spring system may schematically describe a general theoretical model for a compliant wall. The numerical model is quite simple, but the study for this simple model allows us to better appreciate and understand the significance of the hydroelastic-type instabilities in a flow over compliant layer.

Mapping Technique to Detect Absolute Instability

The spatio–temporal evolution of a perturbation impulse located at the origin $x = 0$ is described by the following Green's function:

$$G(x,t) = \frac{1}{4\pi^2}\int_L\int_F \frac{\mathrm{d}\alpha\,\mathrm{d}\omega}{D(\alpha,\omega)}\exp(i\alpha x - i\omega t) \qquad (1)$$

The complex frequency ω and complex wave number α are related by the dispersion relation $D(\alpha, \omega) = 0$. The time-asymptotic response of Green's function may be determined via a process of analytic continuation in which the Laplace contour L is deformed toward the real axis of the complex ω plane. When the Laplace contour L is deformed, the Fourier contour F is simultaneously deformed to preserve the analyticity of the integral if the paths of two α roots originating from opposite halves of the α plane intersect each other. We term such an intersection point a pinch point. The double α roots at the pinch point give rise to a singularity at the corresponding

Received 30 March 2000; revision received 28 September 2000; accepted for publication 23 October 2000.

*Associate Professor, Department of Mechanics; llyzys@public.wh.hb.cn.

†Associate Professor, Department of Mechanical and Production Engineering, Kent Ridge Crescent.